NEUROPATHOLOGY

Neuropathology 2016; **36**, 513–526 doi:10.1111/neup.12302

Original Article

Formation of fibroblastic reticular network in the brain after infection with neurovirulent murine coronavirus

Rihito Watanabe,[1] Masatoshi Kakizaki,[1] Yuzuru Ikehara[2] and Akira Togayachi[2]

[1]Department of Bioinformatics, Graduate School of Engineering, Soka University, Hachioji, Tokyo, Japan and [2]Research Center For Medical Glycoscience, National Institute of Advanced Industrial Science and Technology (AIST), Tsukuba, Ibaraki, Japan

cl-2 virus is an extremely neurovirulent murine coronavirus. However, during the initial phase of infection between 12 and 24 h post-inoculation (hpi), the viral antigens are detected only in the meninges, followed by viral spread into the ventricular wall before invasion into the brain parenchyma, indicating that the viruses employ a passage between the meninges and ventricular wall as an entry route into the brain parenchyma. At 48 hpi, the passage was found to be constructed by ER-TR7 antigen (ERag)-positive fibers (ERfibs) associated with laminin and collagen III between the fourth ventricle and meninges at the cerebellopontine angle. The construct of the fibers mimics the reticular fibers of the fibroblastic reticular network, which comprises a conduit system in the lymphoid organs. In the meninges, ERfibs together with collagen fibers, lining in a striped pattern, made up a pile of thin sheets. In the brain parenchyma, mature ERfibs associated with laminin were found around blood vessels. Besides mature ERfibs, immature Erfibs without associations with other extracellular matrix components like laminin and collagen appeared after infection, suggesting that the CNS creates a unique conduit system for immune communication triggered by viral invasion.

Key words: blood brain barrier, CD11b, extracellular matrix, fibroblastic reticular cell, reticular fiber.

INTRODUCTION

Coronaviruses have relatively high mutation and RNA recombination rates and rapidly undergo cross-species transmission events *in vitro* and *in vivo*.[1–3] In humans, viruses newly emerging out of members of Coronaviridae cause serious diseases, such as severe acute respiratory syndrome (SARS)[4] and Middle East respiratory syndrome (MERS).[5] Interest in the pathogenicity of murine coronaviruses, particularly, mouse hepatitis virus (MHV), has grown because of the high incidences of mutation rates with consequences of different pathogeneses[6–10] as well as their ability, especially in JHM strains of MHV (JHMV), to cause both acute and chronic CNS diseases ,[10,11] because neuropathogenic viruses can induce significant neuronal dysfunction and degeneration of specific neuronal populations, sometimes leading to devastating, life-threatening consequences in infected humans.[12,13] Among JHMVs, cl-2 exhibits extremely high neurovirulence.[10,14,15] A less virulent viral clone, srr7, has been isolated from cl-2, as a soluble receptor-resistant mutant.[16,15] All mice infected with cl-2 die within 3 days post-inoculation (dpi), whereas mice infected with srr7 exhibit no clinical sign before 5 dpi and some of them survive after 10 dpi. However, there is no difference in the viral growth rate during the initial phase of infection between these two strains.[15,17–19] The different virulence of these viruses is attributed to their capability to infect neurons,[15,20] or their infectivity being independent or dependent upon a major MHV-receptor, carcinoembryonic cell adhesion molecule 1.[21,22] In agreement with their similar viral proliferation rates during the early phase of infection, the two viruses exhibit almost the same patterns of viral spread in the brain during the initial phase of infection. The viral antigens are first detected in the infiltrating cells, namely CD11b-positive ($CD11b^+$) cells of monocyte lineage, in the meninges at 12 h post-inoculation (hpi), and not at the site of the inoculation in the frontal lobe.[17,19,23] During 24 to 48 hpi, infected $CD11b^+$ cells appear in the ventricular cavity followed by infection of cell components of the ventricular wall, before viral spread into the brain parenchymal cells.[17,18] The ventricular wall is also the target site during

Correspondence: Rihito Watanabe, MD, Department of Bioinformatics, Graduate School of Engineering, Soka University, 1–236 Tangi-cho, Hachioji, Tokyo 192–8577, Japan. Email: rihitow@soka.ac.jp

Received 08 January 2016; revised 03 March 2016 and accepted 05 March 2016; published online 28 April 2016.

th einitial phase of infection with other species of viruses, including herpes simplex virus[24] and lymphocytic choriomeningitis virus.[25]

The manner of the viral spread after infection with cl-2 or srr7 indicated that there could be some other routes of viral entry into the brain parenchyma than crossing over the blood brain barrier (BBB), which has been almost exclusively studied or hypothesized as the mechanism of neuropathogenic viral entry into the brain parenchyma,[26–30] including a pioneering study of poliovirus using gene-manipulated mice introduced by the human-type polioviral receptor-gene.[31] However, the mechanism of viral distribution of a neurovirulent strain of polioviruses, the Mahoney strain, infecting motor neurons in the CNS, was not elucidated through studies of its ability to circumvent the BBB in comparison with that of an attenuated viral strain, Sabin strain.[32] Our investigation to identify the viral entry route focused on the area between the fourth ventricle (IVv) and meninges in the cerebellopontine angle, because viral antigens are often found in the area during the early phase of infection between 24 to 48 hpi,[17,18] and there is a conduit, the foramen of Luschka, for CSF to flow from the ventricle into the subarachnoid space. Another intriguing feature of viral antigen localization after infection with cl-2 or srr7 is that the viral antigens were found in fibrous structures, which appeared to be the extracellular matrix (ECM), in the brain and spleen.[17,18] Viruses proliferate and produce viral antigens in living cells, and it is unusual to find them in the ECM area through a light-microscopical observation. However, such colocalization of viral antigen or viral particles with the ECM has been reported to occur in the lymphoid organs. After infection with lymphocytic choriomeningitis virus (LCMV), viral antigens are colocalized with the components of reticular fibers, including collagen III and laminin, in the spleen.[33] Similar phenomena have been reported in infection with extremely virulent viruses, such as Ebola,[34] Marburg and Lassa viruses.[35] These viruses infect fibroblastic reticular cells (FRCs) in the lymphoid organs, followed by immune dysfunction leading to viral persistence[33] or tissue destruction.[35]

FRCs are considered to maintain reticular fibers, which compose fibroblastic reticular network (FRN) in the lymph nodes[36–38] and spleen.[39,40] Erasmus University Rotterdam thymic reticulum antibody 7 (ER-TR7) has been used to define FRCs,[41,42,33] although the antigen of ER-TR7 has yet to be determined. Furthermore, there have been no reports on the size or determinant of the antigen using immune reactions, including Western blotting or immunoprecipitation. Each reticular fiber comprising the FRN is around 1 μm in diameter, and contains collagen fibers as a core surrounded by an ER-TR7 antigen-positive ($ERag^+$) microfibrillar layer, and is further enclosed with a basement lamina at the outer surface. The entire fiber is largely ensheathed by FRCs.[43] The FRN functions as a conduit system for immunocompetent cells and inflammation-associated molecules such as cytokines and ligands or foreign antigens to reach appropriate sites in order to cause immune reactions in the lymph nodes[44] and spleen,[39] or to guide homing of the cells.[42,40] Subsequently, FRCs, which are podoplanin (gp38)-positive (Pod^+) and CD31-negative ($CD31^-$), have been reported to co-operate with other stromal cells in the lymph nodes, such as Pod^+ $CD31^+$ lymphatic endothelial cells, Pod^- $CD31^+$ blood endothelial cells, and Pod^- $CD31^-$ myofibroblastic pericytes, to play a key role in the FRN function,[45,46] indicating that there should be organ-specific specialization of the fibroblastic stroma. In this report, we show the virus antigens detected in the brain as fibrous structures colocalized with ERag and laminin as the same images, as previously reported in the spleen infected with LCMV.[33] This finding encouraged us to prove the expression of ERag along the reticular system in the brain, which could function as a scaffold for viral entry and inflammatory cell invasion into the brain.

MATERIALS AND METHODS

Viruses and animals

The highly neurotropic MHV strain MHV-JHM cl-2 (cl-2)[14] was used. This virus was propagated and titrated using DBT cells maintained in Dulbecco's modified Eagle's minimal essential medium (DMEM) (GIBCO, Grand Island, NY) supplemented with 5% fetal bovine serum (FBS) (Sigma, Tokyo Japan), as previously described.[14] Specific pathogen-free inbred BALB/c mice purchased from Charles River (Tokyo, Japan) were maintained according to the guidelines set by the committee of our university. For the experiment with infectious agents, mice were transferred to a biosafety level 3 (BSL-3) laboratory after permission from the committee. At 7–8 weeks old, each mouse was inoculated with 1×10^2 of cl-2 virus into the right frontal lobe under deep anesthesia. As described previously,[17] the scar caused by the needle tip was found in the right frontal lobe after post mortem examination. Between 12 and 72 hpi, organs including the brains and spleens were removed from treated or untreated mice after exsanguination under deep anesthesia. Parts of the organs were embedded in Tissue Tek OCT (Sakura, Tokyo, Japan) and frozen to prepare frozen sections. Remaining portions were processed for viral titration, or fixed in 4% paraformaldehyde buffered with 0.12 mol/L phosphate (PFA) for pathological examination using paraffin-embedded sections to check that each experiment had been appropriately performed as we previously reported using cl-2 for infection,[17,15] and no contradiction was found (data not shown). Some mice were perfused with PFA from the aorta via the left ventricle under deep

anesthesia using diethyl ether and 0.2 mg of chlorar hydrate (Mylan Seiyaku, Tokyo, Japan) per mouse to obtain sections for the detection of dexran labeled with Texas Red, for the three-dimensional construct, or for double or triple immunostaining that includes podoplanin detection.

Immunofluorescence

Ten-micrometer cryostat sections prepared from unfixed frozen tissues were fixed in ice-cold acetone for 10 min. PFA-fixed tissues were rinsed with graded concentrations of sucrose overnight, and processed to prepare cryosections as previously described,[18] which were used without further fixation. Chamber slides with mixed primary culture were fixed either in cold ethanol for 1 min followed by fixation in cold acetone for 5 min, or in PFA for 5 min to perform double or triple immunostaining that includes podoplanin-staining. Immunostaining was carried out using the antibodies and reagents listed in Table 1, as previously described.[18] Fluorescence was visualized with a confocal laser scanning microscope (Leica Microsystems, Heidelberg, Germany) to obtain images of double or triple immunostaining and three-dimensional constructs. A fluorescence microscope (KEYENCE, Osaka, Japan) equipped with a BZ analyzer (KEYENCE) was used for statistical study.

Fluorescent tracers

One mg of 10 kilodalton lysine fixable dextran labeled with Texas Red (Invitrogen Corp., Carlsbad, CA, USA) was injected intravenously in 400 μL of PBS through the tail vein. Ten minutes after the injection, mice were perfused with PFA, the brains and spleens were immersion-fixed overnight in PFA, and then processed for cryosections as described earlier.

Three-dimensional image reconstruction

The PFA-fixed brains were processed either for 40-μm cryosections, or thick sections of 90–150 μm thick, which were prepared by slicing the brain with sharp stainless blades under a dissecting microscope. The cryosections were stained in the same way as the other cryosections described earlier. All procedures to stain the thick sections were performed in a floating state. After rinsing in 0.12 mol/L Tris–HCl

Table 1 List of the staining reagents used

Target (cell type) /antibody	Species	Clone or designation	Conjugate	Source
Primary antibodies				
MHV-JHM	Mouse	Monoclonal		Ref. [20]
MHV-JHM	Rabbit	Polyclonal		Ref. [15]
/ER-TR7	Rat	ER-TR7		AbD Serotec, Oxford, UK
Laminin	Rabbit	Polyclonal		Cosmo Bio Co. Ltd., Tokyo, Japan
Collagen type III	Rabbit	Polyclonal		Acris, San Diego, CA, USA
Podoplanin	Hamster	Monoclonal		AngioBio Co., DerMar, CA, USA
NeuN (Neuron)	Mouse	A60	Biotin	Chemicon, Temecula, CA, USA
Neurofilament	Goat	C-15		Santa Cruz Biotechnology, Santa Cruz, CA, USA
Olig2 (oligodendrocyte)	Rabbit	Polyclonal		Millipore, Temecula, CA, USA
Zic2 (arachnoid cell)	Rabbit	Polyclonal		Millipore
CD11b	Rat	M1/70	Biotin	BD Pharmingen, San Diego, CA, USA
CD13 (pericyte)	Rat	R3-242	FITC	BD Pharmingen
CD31 (endothelial cell)	Rat	390	Biotin	BD Pharmingen
GFAP (astrocyte)	Rabbit	Polyclonal		DAKO, Tokyo, Japan
GFAP (astrocyte)	Mouse	G-A-5		Sigma, Tokyo, Japan
Cytokeratin	Mouse	C-11		Sigma
Secondary antibodies				
Anti-rat IgG	Donkey	Polyclonal	Alexa488	Molecular Probes, Carlsbad, CA, USA
Anti-rabbit IgG	Sheep	Polyclonal	FITC	Abcam, Cambridge, UK
Anti-rabbit IgG	Goat	Polyclonal	Alexa568	Invitrogen, Carlsbad, CA, USA
Anti-goat IgG	Donkey	Polyclonal	Rhodamine	Chemicon
Anti-goat IgG	Donkey	Polyclonal	Alexa488	Invitrogen
Anti-mouse IgG	Goat	Polyclonal	Alexa488	Molecular Probes
Anti-mouse IgG	Donkey	Polyclonal	Biotin	Rockland, Gilbertsville, PA, USA
Anti-hamster IgG	Goat	Polyclonal	Biotin	Jackson ImmunoResearch, West Grove, PA, USA
Biotin		streptavidin	Alexa488	Invitrogen
Biotin		streptavidin	Alexa568	Invitrogen
Biotin		streptavidin	PE-CY5.5	Southern Biotech, Birmingham, AL, USA

MHV-JHM, mouse hepatitis virus strain JHM; NeuN, neuronal nuclei; Olig2, oligodendrocyte lineage transcription factor 2; Zic2, zinc-finger transcription factor 2; FITC, fluorescein isothiocyanate; PE-CY5.5, R-phycoerythrin-cyanine 5.5; Ref., Reference.

(pH 7.4) for 1 h, thick sections were incubated with blocking solutions for 1 h,[18] followed by incubation with primary antibodies overnight. Each of the second and third steps of staining were conducted for 30 min. Three-dimensional images were generated with Leica software (Leica Microsystems, Heidelberg, Germany).

Quantification of immunofluorescence staining

Twenty-four-bit color images with a 1360 × 1024 pixel resolution were acquired with a fluorescence microscope (KEYENCE). Three independent approaches were performed to quantify the observed immunofluorescence signal using the BZ analyzer. The background fluorescence intensity (FI) in areas of the field of view was subtracted from total measurements of FI. The average fluorescence intensity (AFI) within the unit area was obtained by dividing its integrated FI by its area.

RESULTS

Expression of ERag after viral infection

An increased level of ERfibs in the restricted area of the brain was already detectable at 12 hpi with cl-2 (Fig. 1A–C), with an increased and intense staining for ERfib compared with that of an uninfected mouse (Fig. 1B) or sham infected mouse (Fig. 1C) in the root of the trigeminal nerve, especially in the area where GFAP-positive activated astrocytes were observed near the border with the peripheral nervous system (Fig. 1A3). A more extended distribution of ERfibs was observed during the later phase of infection (Fig. 1D, E). Furthermore, virus antigens in fibrous structures reported in our previous study[17,18] were found to colocalize with laminin and ERag (Fig. 1F) with almost the same image observed in the spleen of mice infected with LCMV,[33] which indicated that viruses are concentrated in the narrow space of reticular fibers[33,43] and are recognized by immunofluorescence, and they use the reticular conduit system as a scaffold.[33,35] In order to quantify the increase and association of ERfibs with laminin, the average fluorescence intensity (AFI) of divided areas ($0.9–2.4 \times 10^4$ μm^2) was measured in sections which included the pons (Fig. 2A). There was a high positive correlation of the distribution and intensity between laminin and ERag expression in an untreated mouse (R^2 = 0.82) and virally infected mouse at 48 hpi ($R^2 = 0.78$, Fig. 2A), as well as an increase of the expression at 48 hpi with cl-2 compared with that at 12 hpi (Table 2). The laminin expression of the mouse at 12 hpi with cl-2 was more rapid compared with the ERag expression, and was more extensive at 48 hpi than those of medium or untreated mice (Table 2).

Next, a detailed study of AFI in the area around the foramen of Luschka, which provides a conduit for CSF between the fourth ventricle and subarachnoid space at the cerebellopontine angle, was performed, because the viral antigens are initially detected in inflammatory cells that have infiltrated the meninges, followed by inflammatory cells in the ventricular cavity and cell components of the ventricular wall.[17,18] AFIs in the dotted areas in Figure 3E were compared among those of cl-2-, sham-infected and untreated mice (Fig. 2B). Because of variable AFI levels in individual mice, especially in infected mice showing high SDs, a significant increase of AFI in the area of cl-2-infected mice compared with that of sham-infected mice at 48 hpi was obtained in the deeper area of the fourth ventricle, 300–500 μm inside from the outermost portion of the lateral recess of the fourth ventricle (OV) (Fig. 2B). At 72 hpi, the expression of ERfib remained at high levels in cl-2-infected mice, whereas the relatively high levels in the outer areas of the lateral recess of sham-infected mice at 48 hpi decreased at 72 hpi to the levels of untreated mice (Fig. 2B). The expression of ERag was either colocalized with that of components of the extracellular matrix (ECM) such as laminin (Fig. 1D) and collagen (Fig. 1E) in the same way as reticular fibers reported in lymphoid organs,[33] or found without such colocalization as shown in the brain parenchyma (Fig. 1D2 and D3) and trigeminal root (Supplemental Figure S1A). In the ventricle, we also found ERag without an association with other ECM (Figs 1E and 4D), which indicated that there could be immature ERfibs formed during initial events of the host reaction, compared with the mature form of $ERag^+$ reticular fibers associated with several kinds of ECMs observed in lymphoid organs.[33,45,47] Therefore, we compared the length of ERfibs colocalized with laminin in the ventricle between those of infected and sham infected mice, and found a greater difference between those in the two groups (Fig. 2C) than on comparison of ERfibs alone.

$ERag^+$ structure as a conduit in the brain

In order to examine whether the expression of ERfib plays a role as a conduit system in the ventricle as reported in the spleen and lymph node,[39,44] fluorescence-labeled dextran was intravenously injected. Mice infected with the virus showed the infiltration of many particles of dextran along with ERfibs into a deep area in the ventricle (Fig. 3A and Supplemental Figure S1B). A few dextran particles were detected in the hilum of the ventricle near the border with the meninx of sham-infected mice (Fig. 3B), and no trace of the particles was seen in the ventricles of mice with no treatment (Fig. 3C). The dextran particles were appropriately introduced into the recipients, because a high level of the particles was seen in the spleen of mice with no treatment along with Erfbs, especially in the marginal zone around the follicle (Fig. 3D), and partially in the follicle (insert in Fig. 3D), as previously reported.[39] The viral antigens were detected in the ventricle of cl-2-infected mice in a similar way as

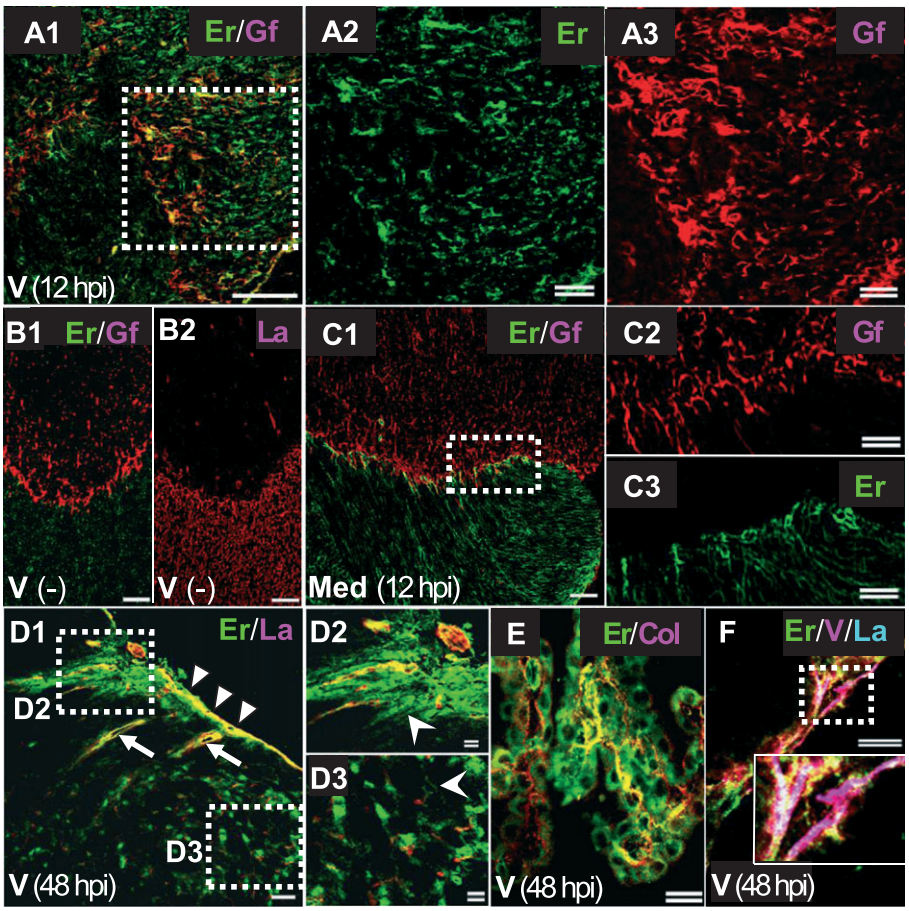

Fig. 1 Frozen sections were prepared from the root of the trigeminal nerve (A C) and pons (D F) of untreated mice (V(-)), mice sham-infected with medium at 12 hours post-infection (hpi) (Med (12 hpi)), or mice infected with cl-2 at 12 and 48 hpi (V (12 hpi) and V (48 hpi), respectively). Immunostaining was performed using ER-TR7 antibody (Er), anti-GFAP (Gf), anti-laminin (La), anti-collagen III (Col), and anti-JHM strains of mouse hepatitis virus (anti-JHMV) (V) antibodies. A: Both in the areas of the peripheral nerve (lower left) and CNS (upper right with prominent astrocytic activation (A3)), the expression of ER-TR7 antigen (ERag) was detected. The dotted area in A1 is shown at higher magnifications (A2 and A3). The orientation of this area is shown at a lower magnification in Supplemental Figure S1A2. B: A low level of ERag was detected (B1) especially in the area of the peripheral nerve (GFAP-negative lower area). The area of the peripheral nerve is shown as a laminin-positive area in the serial section (B2). C: Moderately more intensive staining of ERag was observed in the sham-infected mouse than in the uninfected mouse. The boxed area is shown at a higher magnification (C2 and C3). In the area of the peripheral nerve (lower area), ERag was not colocalized with laminin (Supplemental Fig. S1A), although, in the peripheral nervous system, there were abundant amounts of laminin (B2) comprising the basement lamina around Schwann cells. D: At 48 hpi with cl-2, ERag colocalized with laminin around the blood vessels (arrows) and meninx (triangles) became prominent. Away from the blood vessels and meninx, $ERag^+$ areas without such colocalization were distributed. Higher magnifications (D2 and D3) of boxed areas in D1 show that some areas of the $ERag^+$ laminin arrangement exhibit cellular structures, and some fibrous configurations (arrowhead). E: ERag and collagen III, in the fourth ventricle. F: Colocalization of laminin, collagen III and the viral antigens in the meninx around the pons is shown in white. Single and double bars indicate 50 and 20 μm, respectively.

dextran particles. In the deeper area of the ventricle at the positions corresponding to b and c in Figure 3E, viral antigen-positive cells closely associated with ERfibs were observed (Fig. 3G and H, respectively). However, in the area near the junction between the meninges and ventricle at position a in Figure 3E, the viral antigens did not always distribute along with ERfibs (Fig. 3F), possibly because viruses brought into the ventricle earlier than in the deeper area had time to induce the antigens in the infiltrated and domestic cells after infection. Because viral antigens are already detectable in cells of the monocyte lineage (MoCs) that have infiltrated the meninges during the initial phase of infection at 12 hpi,[17] CD11b-positive ($CD11b^+$) cells as a carrier to transport viruses into the ventricle were examined. Double staining for CD11b and ERag revealed a close association of MoCs and ERfibs in the ventricle (Fig. 3I). As expected, many of the $CD11b^+$ cells in the ventricle were infected (Fig. 3J).

Three-dimensional reconstruction of ERag-positive structure

In order to study stereostructures of ERfbs, we three-dimensionally reconstructed consecutive confocal images

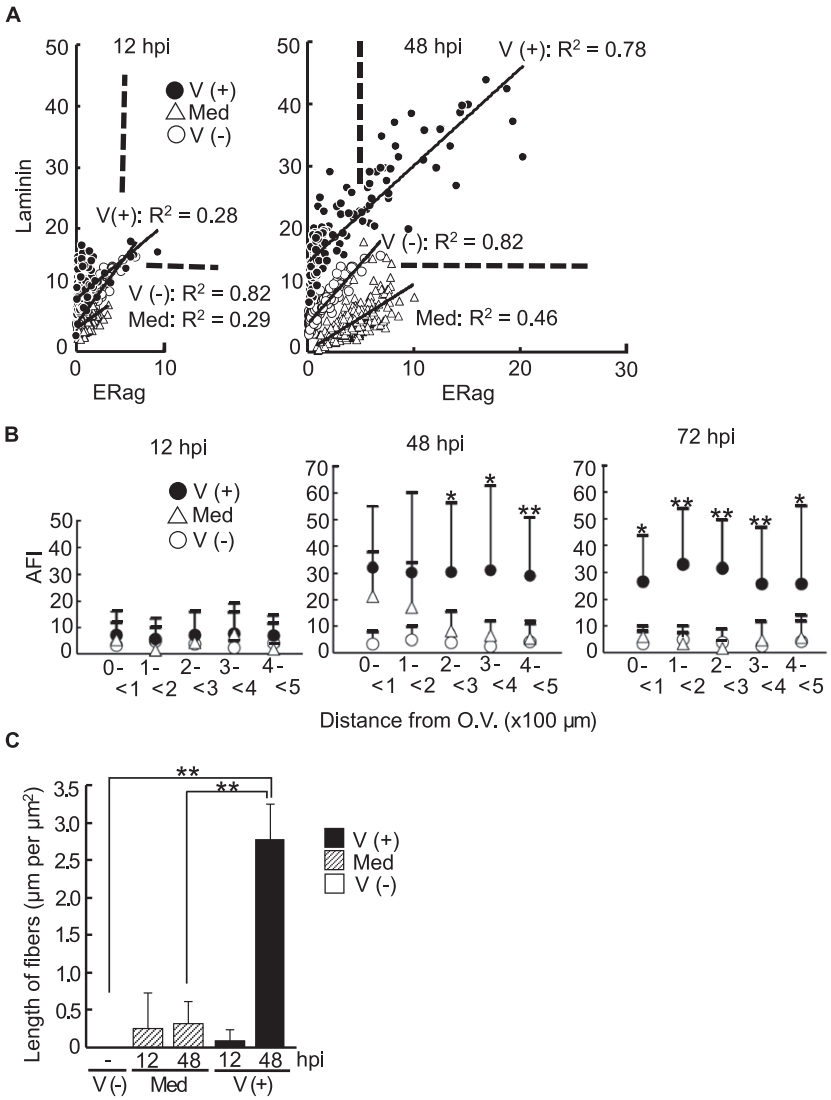

Fig. 2 Average fluorescence intensity (AFI) of ER-TR7 antigen (ERag) and laminin (A and B) or average length of ERag-positive fibers (ERfibs) colocalized with laminin (C) were measured in frozen coronal sections at the level of the foramen of Luschka (A C). Mice were inoculated with cl-2 (V+) or medium (Med), or untreated (V-), and were processed for measurement at 12, 24, 48 or 72 hours post-inoculation (hpi). A: The entire area of the pons was divided into 140 240 areas, and AFI is shown as the fluorescence intensity (FI) in each area per pixel. Results shown are from one mouse for each treatment and are representative of three independent experiments. The square of the correlation coefficient, R^2 is indicated in the graph. The upper and left sides of the horizontal and vertical dotted lines, respectively, show 2% of the total area measured in the untreated mouse. A comparison of AFIs among mice of each treatment is summarized in Table 2. B: The area in the fourth ventricle (IVv) including the space and ependymal cell layers was divided into five areas between the outermost portion of the lateral recess of the IVv (OV) and 500 μm distant from OV. AFI of ERag is shown as FI of each area per pixel obtained from three independently treated mice for each group. Vertical lines indicate SD. C: The average length per μm^2 of ERag-positive fibers associated with laminin expression in IVv obtained from three independently treated mice for each group. Vertical lines indicate SD. * and ** indicate the *P*-value (*P*) examined by Student's *t*-test <0.05 and <0.005, respectively.

of 40 μm-thick sections of the brains. The integrated intensity of immunofluorescence of 35 slices of a 1.5 μm thickness showed robustly stained fibrous structures with a more than 5 μm thickness in the meninx (Fig. 4A) and ventricle (Fig. 4E), which were double-stained for ERag and collagen or laminin, respectively. In the meninx, most of the ERfbs seemed to localize together with collagen based on the view of the integrated image (Fig. 4A). However, rotation of the image revealed a sheet composed of ERfbs and collagen fibers in a fine striped pattern (Fig. 4C and Supplemental movie S1). At the meninx with inflammation, many cells were observed, after triple staining for the nucleus, ERfibs and collagen, in the narrow space between the sheets composed of an association of ERfibs and collagen (Fig. 4B). Another finding obtained from three-dimensional analysis was that a hammock-like structure composed of fine ERfbs

Table 2 Average fluorescence intensity (AFI) of ER-TR7 antigen (ERag) and laminin

	Laminin (%)							
hpi	12		12 (high)		48		48 (high)	
V(+)	12.7	(15.2±1.2)	3.6	(16.6±0.8)	80.6	*(21.5±7.6)	63.2	(23.4±12.4)
Med	0.0	n	0.0	n	1.7	(15.7±1.6)	0.4	(17.9)
V(-)	2.0	(14.7±0.9)	0.0	n	2.0	(14.7±0.9)	0.0	n
	ERag (%)							
hpi	12		12 (high)		48		48 (high)	
V(+)	3.0	(6.9±1.4)	0.6	(9.3)	24.5	*(9.9±4.3)	17.4	**(11.6±4.0)
Med	0.0	n	0.0	n	25.8	(6.4±1.0)	7.9	(7.7±0.7)
V(-)	2.0	(5.8±0.9)	0.0	n	2.0	(5.8±0.9)	0.0	n

Average fluorescence intensity (AFI) of ERag and laminin in the pons of mice inoculated with cl-2 (V+), medium (Med) at 12 and 48 hpi, or untreated (V-), shown in Fig. 2A is summarized as percent positive population of areas (%) for each treatment. Positive populations were defined as those with an AFI of >13.8 or 5.1 in laminin or ERag staining, respectively (horizontal or vertical dotted lines in Fig. 2A, respectively), where 2% of the population measured in (V-) mouse were found. When AFIs are higher than the highest AFI measured in the (V-) mouse, which corresponds to an AFI of >15.4 or 6.8 in laminin or ERag staining, respectively, that was defined as highly positive (high). hps, hours post-infection; n, no matched areas. Figures in the parentheses are mean ± SD, and the figures without ± show that one area was counted under the term. The significance of the difference was analyzed by Student's *t*-test, with *P*-value shown. $^{*}P < 0.005$, V (12 hpi) vs. V (48 hpi); $^{**}P < 0.005$, Med versus V (48 hpi).

hanging on bold lines of laminin, which were partially colocalized with Erfibs, was formed in the ventricle (Fig. 4E and Supplemental movie S2), which could have been ignored on non-specific staining based on typical confocal images of two dimensions because of their overly faint staining.

ERag-producing cells in the brain

In the meninges, arachnoid cells with the expression of cytokeratin or Zic2 showed colocalization with ERag (Fig. 5C, D). Arachnoid cells are reportedly podoplanin-positive (Pod^+),[48] just as with FRCs in the lymphoid organs.[45–47] However, in our analysis, only part of $Zic2^+$ cells in the meninges was Pod^+ (Supplemental Fig. S1C). A thick Pod^+ layer in the meninges was colocalized with ERag (Fig. 5B), most of which could be produced by fibroblasts, which are located in the meninges.[49] Some podoplanin-negative (Pod^-) cells (arrowheads in Fig. 5B) as well as structures making up the basal area (arrows in Fig. 5B) of meninges were also found to be $ERag^+$. In the ventricle, some of the ependymal cells with cytokeratin expression were found to produce ERag. In the brain parenchyma, many GFAP-positive astrocytes, especially those comprising glia limitans at the brain surface (Fig. 5F), or near the border with the peripheral nerve (Fig. 1C), were found to be $ERag^+$. Deep in the parenchyma, $ERag^+$ astrocytes were observed around the blood vessel (Fig. 5G). However, in the brain parenchyma, many $ERag^+$ cells without colocalization with laminin (Fig. 1D3), which were not located around the blood vessels, were seen. Furthermore, astrocytes situated away from blood vessels deep in the brain parenchyma, even though they had contact with $ERag^+$ cells, did not produce ERag (Supplemental Fig. S1D). Therefore, we examined other cell types which produce ERag in the brain parenchyma, and found $ERag^+$ neurons and oligodendrocytes (Fig. 5H, I), in addition to endothelial cells (Fig. 5J) and pericytes (Fig. 5K) of blood vessels (Bv) in the brain parenchymal area (PaBv). However, brain parenchymal $CD11b^{low}$ cells (arrowheads in Supplemental Fig. S1E), possibly microglia,[50] as well as infiltrating $CD11b^{high}$ cells in the meninges (arrows in Supplemental Fig. S1E) and ventricle (Fig 3I) were $ERag^-$. In addition, $ERag^+$ cells distributed in the area away from the viral antigen-positive site (Fig. 5L) indicated that the signal of viral entry reached these $ERag^+$ cells via an undetermined pathway.

DISCUSSION

A classical neuropathology states that, in the brain in the presence of infectious diseases, there is an increase in reticular fibers, detected by silver staining, and these fibers are associated with inflammatory cells.[51] A recent study also detected an increase of reticular fibers as second harmonic generation structures in toxoplasmic encephalitis (TE).[52] Although the modern sophisticated technique revealed a three-dimensional structure of the reticular network, which may be used as a scaffold for antigen-specific T cells to

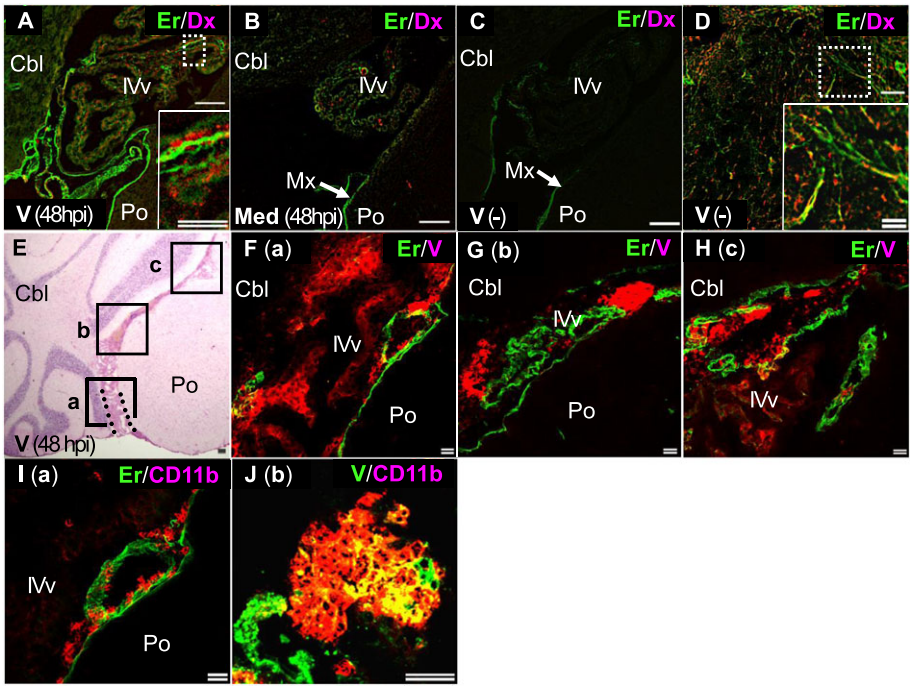

Fig. 3 A D: Mice infected with cl-2 or sham-infected with medium at 48 hours post-inoculation (hpi) (V (48 hpi)) or (Med (48 hpi), respectively), or untreated mice (V(-)), intravenously received dextran labeled with Texas red (Dx). Frozen sections were prepared to visualize ER-TR7 antigen (ERag) (Er) by immunofluorescence. Dextran particles along with ERag-positive fibers (ERfibs), observed in the deep area of the ventricle of the cl-2-infected mouse and shown at a higher magnification as an insert in A, reached the middle portion of the fourth ventricle (Supplemental Figure S1 B), the area which corresponds to the boxed area c in E. In the untreated mouse, only low levels of dextran particles were observed in the choroid plexus facing the meninx (C), although many were traceable even in the follicle (dotted area in D) of the spleen along with ERfibs, in the same manner as previously reported.[39] E J: The brain of the mouse infected with cl-2 was snap-frozen to prepare serial frozen sections for HE (E) and immunofluorescence (F J) staining using ER-TR7, anti-JHM (V), and anti-CD11b (CD11b) antibodies. Note that there are no marked destructive changes detectable at a low magnification at 48 hpi with cl-2 (E). The viral antigens are more closely associated with ERag in the deeper position in the ventricle (H) than in the hilum (F). $CD11b^+$ cells are closely associated with ERag (I). The viral antigens are predominantly detected in the $SD11b^+$ cells (J). The letters in parenthesis in F J indicate the corresponding areas in E of each area chosen for the image. Cbl, Po, VIv and Mx indicate the cerebellum, pons, fourth ventricle and meninx, respectively. Single and double bars in (A–D, F J) indicate 50 and 20 μm, respectively; scale bar in (E) indicates 100 μm.

migrate into the infected sites in the brain, questions that were raised half a century ago[51] (What are the components of the reticular fibers, and which cells in the CNS produce the components?), still remain to be answered.[52] In this report, we showed ERfibs as one of such components, which increase during infection and comprise a reticular network unique to the brain (BrRN) but in part analogous to FRN in the lymphoid organs, detected as $ERag^+$ fibrous structures and forming a conduit system .[39,44,45]

$ERag^+$ structures have been detected in the brains after infection[52,53] or physical treatment,[49] and in the retina of gene-manipulated mice,[54] as well as in normal mice at low basal levels in the meninges[49,52] and basement membrane of blood vessels.[52] In these reports, ERag was used as a marker of reticular fibroblasts, although the figures in the papers show the co-localization of ERag and GFAP ,[49,54] and the contribution of ERfibs to immune-mediating communication or a scaffold is not mentioned. One of the reasons that such an important role of ERfibs to operate a conduit system in other organs was not described could be that the authors might have been obliged to limit the character of $ERag^+$ structures, because an increase of these structures in injured regions, which were examined at around 1 week or more after the treatment of the mice, might not be large enough to trace and prove that they function as a conduit system. For example, $ERag^+$ structures in the meninges have been reported to be found only in the sulcus[52] where the arachnoid membrane does not exist. In contrast, our results showed high expression of $ERag^+$ structures in the arachnoid membrane. The reason why we could trace the ERfibs could be that the virus cl-2 is an extremely neurovirulent strain, leading infected mice to a morbid state in 48 hpi.[8,9,14] The more vigorous the insult is, the more extended the host reaction would be. Actually, the increased thickness of the arachnoid membrane formed during concentrated time periods after the infection enabled us to observe the architecture of a striped pattern consisting of ERfibs and collagen fibers, forming the sheet of a thin membrane. Each of the sheets was approximately 0.7–1.0 μm thick, which corresponds to the diameter of each reticular

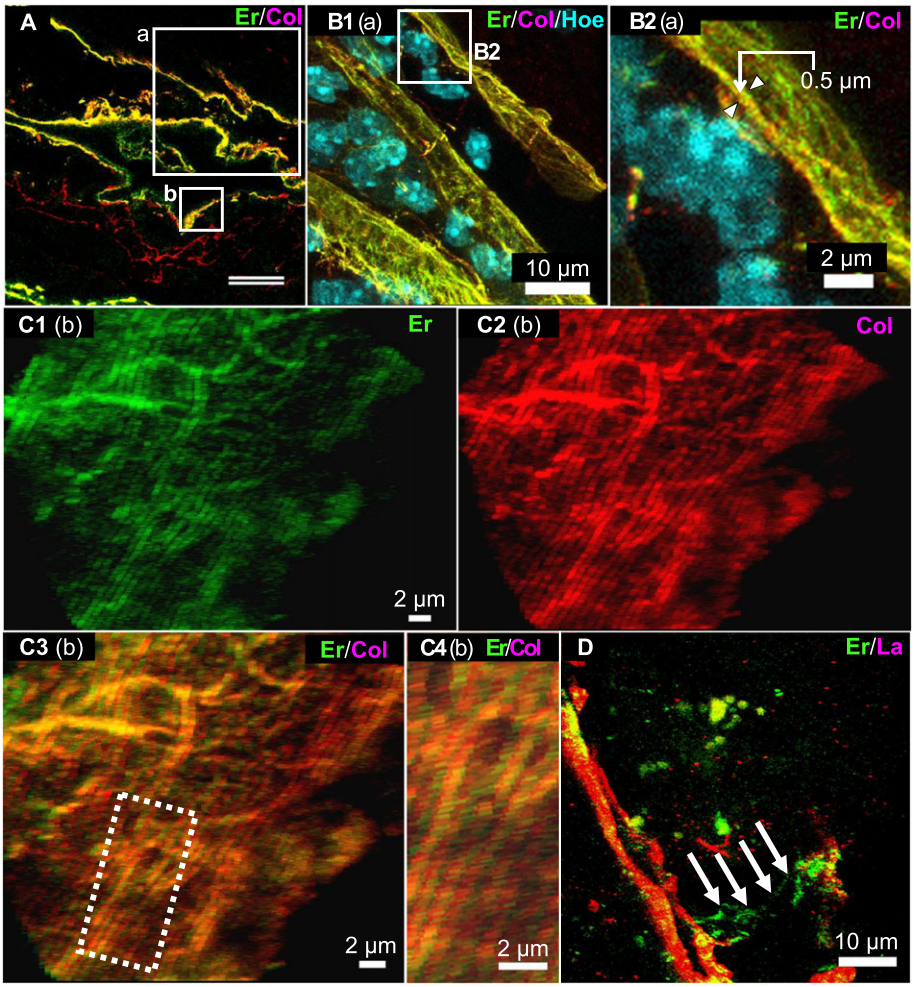

Fig. 4 Three-dimensional images were constructed after staining ER-TR7 antigen (ERag) (Er) and collagen III (Col) in the meninges of the cerebellopontine angle (A D), or laminin (La) in the fourth ventricle (E) of a mouse infected with cl-2 at 48 hours post-infection (hpi). Nuclear counter-staining was performed using Hoechst 33342 (Hoe). The letters in parenthesis in B,C indicate the areas of images corresponding to the boxed areas in A. Between the sheets, many cells were found to be packed (B1). The thickness of the sheet was estimated at around 0.5 1.0 μm after viewing the sheet from a different angle (B2 and Supplemental Figure S2). The rotation of images around the Y axis disclosed sheet structures (Supplemental Movie S1) composed of ERag-positive fibers (ERfibs) and collagen fibers (C and D at a higher magnification of the dotted area in C3). The ventricle contained a fine ERag$^+$ structure without colocalization with laminin (arrows in E) after the rotation of images (Supplemental Movie S2). The double bar in A indicates 20 μm. Single bars indicate 2 μm (B2 D) and 10 μm (B1 and E).

fiber serving as a unit of the conduit system in the lymphoid organs,[43,45] and the sheets had been considered to be meningeal fibers on the two-dimensional observation of thin sections. Furthermore, between the sheets, many cells were detected, many of which should be infected CD11b$^+$ cells.[17,18] A classic neuropathological understanding of the sites of infiltrating cells observed in meningitis has theoretically assumed a subarachnoid space between the arachnoid membrane and pia mater. The ERfib-embedded sheets may guide inflammatory cells after extravasation to migrate into the meningeal region, but on the other hand, the sheets might restrict the inflammatory lesion in the meninx blocking the direct spread of inflammatory cells and viral particles from the meninx into the brain parenchyma. At least at 48 hpi, the prevention of direct invasion of the inflammatory cells and viruses from the meninx to the brain parenchyma seemed to be successful, as has also been observed in meningitis induced by other infectious agents.[55–57] Before our findings, such prevention was thought to be operated by the pia mater and astrocytes comprising glia limitans at the brain surface,[58] because inflammatory cells and infectious agents have been considered to be able to freely move around the presumed subarachnoid space.

The increase in ERfibs after infection had already occurred at 12 hpi. However, the possibility that all of the newly formed ERfibs function analogous to FRN in the lymph nodes and spleen is not conceivable, because invasions of CD11b$^+$ cells and viruses into ERag-upregulated areas were not prominent at 12 hpi. In addition, although ERfibs in the fourth ventricle, especially near the area of

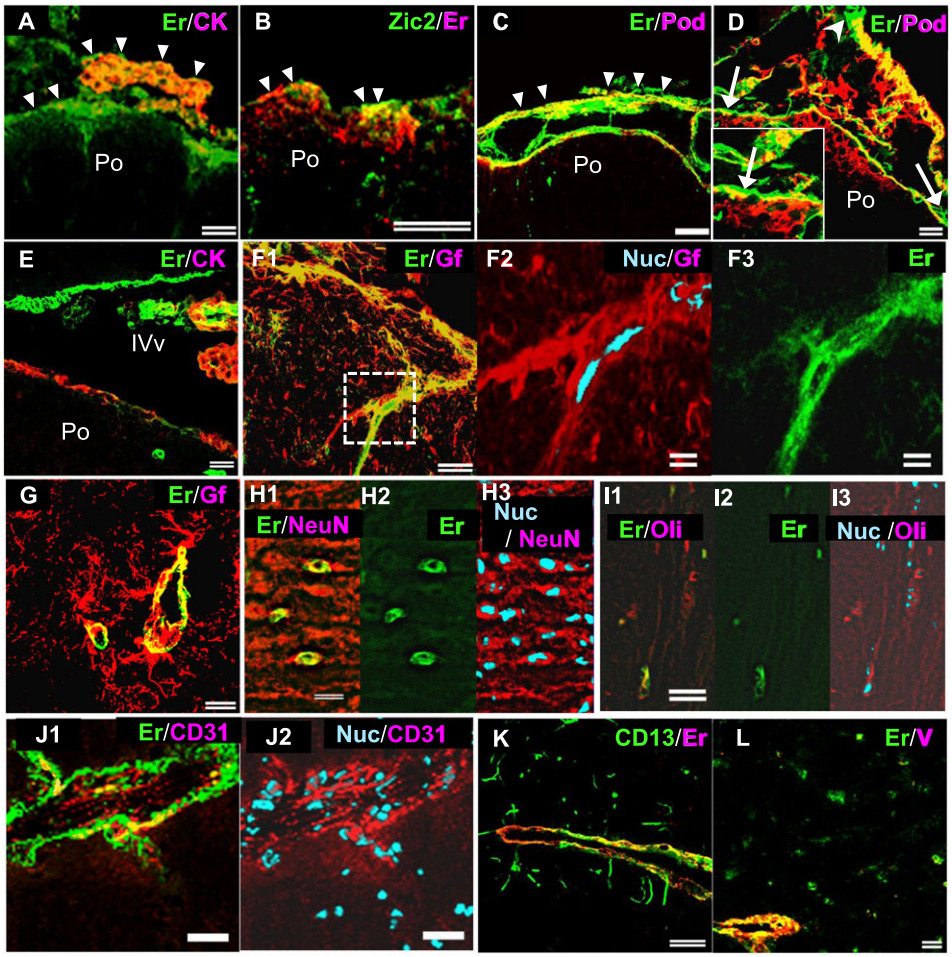

Fig. 5 Frozen sections prepared from the meningeal areas (A D), ventricular area (E) and parenchymal areas of the pons (F L) of mice infected with cl-2 at 48 hours post-infection (hpi) underwent staining for ER-TR7 antigen (ERag) (Er), cytokeratin (CK), Zic2, podoplanin (Pod), GFAP (Gf), JHM strains of mouse hepatitis virus (JHMV) (V), neuronal nuclei (NeuN), oligodendrocyte lineage transcription factor 2 (Oli), CD31 and CD13 antigens, and nuclear counter-staining (Nuc) by immunofluorescence. A E: Arachnoid cells shown as CK-positive (CK^+) and Zic-2^+ and ependymal cells shown as CK^+ cells produced ERag. Pod is reportedly expressed in arachnoid cells,[48] but only a part of $Zic2^+$ cells were Pod^+ (Supplemental Fig. S1C, respectively). F and G: Astrocytes producing ERag at the brain surface making up glia limitans (F), and those deep in the brain parenchyma, where astrocytes around the blood vessels (PaBvs) produce ERag (G), but not those distant from PaBvs, even in the area with many ERag-producing parenchymal cells (Supplemental Fig. S1D). The dotted area in F1 is shown at a higher magnification in F2 and F3. H K: CNS components other than astrocytes produced ERag, such as neurons (H), oligodendrocytes (I), endothelial cells (J), and pericytes (K). However, neither $CD11b^{high}$ nor $CD11b^{low}$ cells produced ERag (Supplemental Fig. S1E). Triangles and IVv indicate the meninges and fourth ventricle, respectively. Single and double bars indicate 50 and 20 μm, respectively.

the junction of the ventricle and meninx, were increased in sham-infected mice compared with non-treated mice, fluorescence-labeled dextran particles, which have been used as tracers to show the function of FRNs in the spleen,[39] were not detected in the fourth ventricle. In contrast, in cl-2-infected mice, labeled dextran particles were found in the ventricle showing a close association with Erfibs. This and subsequent findings indicated that ERfibs need to be allied with some other substances including ECM components detected in FRN to function as a scaffold. The ERfibs in the ventricle of infected mice were co-localized with laminin at a higher level compared with those of sham-infected mice. In addition, ERfibs that appeared at 12 hpi were not co-localized with laminin, although in the area of peripheral nerves there were high levels of pre-existing laminin as a component of the basement membrane around Schwann cells. Another immature form of ERfibs appeared after the three-dimensional construction of images. In the fourth ventricle, an $ERag^+$ net-like structure was found hanging on two pole-like structures of laminin, without forming firm fibers. The findings were supported by a study using a primary brain mix culture, where several stages of $ERag^+$ expression with various types of association with ECM were observed (data not shown). Besides collagen and components of the basement lamina including laminin,[43] several kinds of molecules, such as decorin, biglycan and fibromodulin, which are surrounded by the $ERag^+$ matrix and localized to the conduit core,[45] are supposed to be engaged in the maturation

of FRN with the ERag$^+$ matrix to function as a conduit in the lymph nodes. In addition, FRCs, a core cell population to maintain the ECM and conduit system in the lymph nodes, produce large amounts of other molecules involved in the matrix and elastic fiber assembly, including lysyl oxidase (LOX), LOX-like 1, microfibril-associated glycoprotein 2 (MFAP-2), MFAP-5 and fibulin-1.[45] Future studies should elucidate the roles of these factors in regulating the reticular network in the brain.

FRCs are thought to be highly specialized to the lymphoid microenvironment.[45,59] In order to study the corresponding cell population in the brain, we investigated cells that produce ERag, which is one of the whole markers of FRCs and FRN .[33,40,41] Besides expected cell populations such as Pod$^+$ ERag $^+$ cells in the meninges, various types of cells in the brain showed ERag expression, including arachnoid cells, ependymal cells, endothelial cells and pericytes, which were judged through the expression of representative cell marker proteins, their localization in the tissue and their shape. In addition, to our surprise, all kinds of the brain parenchymal cells except for CD11b^{low} cells, provbably microglia, showed ERag expression. In spite of these findings, it is not plausible that the ERag produced by brain parenchymal cells was directly employed in the conduit system to guide the invasions of the virus or inflammatory cells, as indicated in the meninges and ventricle, because the viral antigens and inflammatory cell invasions were not observed at 48 hpi in the large area where they were produced by brain parenchymal cells. Furthermore, most of them were not colocalized with laminin fibers, except for the close association of GFAP$^+$ and laminin$^+$ fibers around the blood vessels, where the basement membrane is formed facing astrocytes at the side of blood vessels even under normal conditions.[26] However, the colocalization of ERag and laminin$^+$ fibers around the blood vessels was detected. The results indicate that a conduit system could be created around the PaBv, because information that virus-bearing CD11b$^+$ cells had invaded the meninges and ventricle must reach to the area with ERag expression in the brain parenchyma.

The conduits in the lymphoid organs are able to transfer such information through micro- and macromolecules, including cytokines and ligands.[36,39] In the brain, foot processes of astrocytes, neurons and microglia adhere to the basement lamina around the blood vessels.[26,60] When the information reaches the cells around the blood vessels, cell-to-cell-mediated immune cross-talk through an immune synapse reported in lymphoid cells,[61] and /or the use of not only immune-related molecules but also several neurotransmitters as a tool,[62] could possibly trigger an immune reaction in the brain parenchymal cells distant from blood vessels. Astrocytes might play such a role in cellular communication because of their ability to produce high levels of ERag and their localization around the blood vessels, ventricles and brain surface. Therefore, local immune reactions relevant to brain pathology should be further examined, especially on cross-talk between brain parenchymal cells,[63] possibly after receiving information from the conduit around the PaBv.

ACKNOWLEDGMENTS

This work was supported in part by grants from the Ministry of Education, Culture, Sports, Science and Technology Grant Number: 22 590 368).

REFERENCES

1. Baric RS, Yount B, Hensley L, Peel SA, Chen W. Episodic evolution mediates interspecies transfer of a murine coronavirus. *J Virol* 1997; **71**: 1946–1955.
2. Baric RS, Sullivan E, Hensley L, Yount B, Chen W. Persistent infection promotes cross-species transmissibility of mouse hepatitis virus. *J Virol* 1999; **73**: 638–649.
3. Tresnan DB, Levis R, Holmes KV. Feline aminopeptidase N serves as a receptor for feline, canine, porcine, and human coronaviruses in serogroup I. *J Virol* 1996; **70**: 8669–8674.
4. Kawase M, Shirato K, van der Hoek L, Taguchi F, Matsuyama S. Simultaneous treatment of human bronchial epithelial cells with serine and cysteine protease inhibitors prevents severe acute respiratory syndrome coronavirus entry. *J Virol* 2012; **86**: 6537–6545.
5. de Groot RJ, Baker SC, Baric RS *et al.* Middle East Respiratory Syndrome Coronavirus (MERS-CoV); Announcement of the Coronavirus Study Group. *J Virol* 2013; **87** (14): 7790–7792.
6. Butler NS, Theodossis A, Webb AI *et al.* Structural and biological basis of CTL escape in coronavirus-infected mice. *J Immunol* 2008; **180**: 3926–3937.
7. Saeki K, Ohtsuka N, Taguchi F. Isolation and characterization of murine coronavirus mutants resistant to neutralization by soluble receptors. *Adv Exp Med Biol* 1998; **440**: 11–16.
8. Nomura R, Kashiwazaki H, Kakizaki M, Matsuyama S, Taguchi F, Watanabe R. Receptor-independent infection by mutant viruses newly isolated from the neuropathogenic mouse hepatitis virus srr7 detected through a combination of spinoculation and ultraviolet radiation. *Jpn J Infect Dis* 2011; **64**: 499–505.
9. Kakizaki M, Kashiwazaki H, Watanabe R. Mutant murine hepatitis virus-induced apoptosis in the hippocampus. *Jpn J Infect Dis* 2014; **67**: 9–16.
10. Bender SJ, Phillips JM, Scott EP, Weiss SR. Murine Coronavirus Receptors Are Differentially Expressed in the Central Nervous System and Play Virus Strain-Dependent Roles in Neuronal Spread. *J Virol* 2010; **84**: 11 030–11 044.

11. Flory E, Stuhler A, Barac-Latas V, Lassmann H, Wege H. Coronavirus-induced encephalomyelitis: balance between protection and immune pathology depends on the immunization schedule with spike protein S. *J Gen Virol* 1995; **76** (Pt 4): 873–879.
12. Amor S, Puentes F, Baker D, van der Valk P. Inflammation in neurodegenerative diseases. *Immunology* 2010; **129**: 154–69.
13. Girard S, Couderc T, Destombes J, Thiesson D, Delpeyroux F, Blondel B. Poliovirus induces apoptosis in the mouse central nervous system. *J Virol* 1999; **73**: 6066–6072.
14. Taguchi F, Siddell SG, Wege H, ter Meulen V. Characterization of a variant virus selected in rat brains after infection by coronavirus mouse hepatitis virus JHM. *J Virol* 1985; **54**: 429–435.
15. Matsuyama S, Watanabe R, Taguchi F. Neurovirulence in mice of soluble receptor-resistant (srr) mutants of mouse hepatitis virus: intensive apoptosis caused by less virulent srr mutant. *Arch Virol* 2001; **146**: 1643–1654.
16. Saeki K, Ohtsuka N, Taguchi F. Identification of spike protein residues of murine coronavirus responsible for receptor-binding activity by use of soluble receptor-resistant mutants. *J Virol* 1997; **71**: 9024–9031.
17. Takatsuki H, Taguchi F, Nomura R *et al.* Cytopathy of an infiltrating monocyte lineage during the early phase of infection with murinecoronavirus in the brain. *Neuropathology* 2010; **30**: 361–371.
18. Kashiwazaki H, Nomura R, Matsuyama S, Taguchi F, Watanabe R. Spongiform degeneration induced by neuropathogenic murine coronavirus infection. *Pathol Int* 2011; **61**: 184–191.
19. Kashiwazaki H, Kakizaki M, Ikehara Y, Togayachi A, Narimatsu H, Watanabe R. Mice lacking alpha1,3-fucosyltransferase 9 exhibit modulation of in vivo immune responses against pathogens. *Pathol Int* 2014; **64**: 199–208.
20. Nakagaki K, Taguchi F. Receptor-independent spread of a highly neurotropic murine coronavirus JHMV strain from initially infected microglial cells in mixed neural cultures. *J Virol* 2005; **79**: 6102–6110.
21. Watanabe R, Matsuyama S, Taguchi F. Receptor-independent infection of murine coronavirus: Analysis by spinoculation. *J Virol* 2006; **80**: 4901–4908.
22. Matsuyama S, Taguchi F. Receptor-induced conformational changes of murine coronavirus spike protein. *J Virol* 2002; **76**: 11 819–11 826.
23. Kakizaki M, Togayachi A, Narimatsu H, Watanabe R. Contribution of Lewis X carbohydrate structure to neuropathogenic murine coronaviral spreads. *Jpn J Infect Dis* 2016. DOI:10.7883/yoken.JJID.2015.499.
24. Kopp SJ, Banisadr G, Glajch K *et al.* Infection of neurons and encephalitis after intracranial inoculation of herpes simplex virus requires the entry receptor nectin-1. *Proc Natl Acad Sci U S A* 2009; **106**: 17 916–17 920.
25. Nayak D, Johnson KR, Heydari S, Roth TL, Zinselmeyer BH, McGavern DB. Type I interferon programs innate myeloid dynamics and gene expression in the virally infected nervous system. *PLoS Pathog* 2013; **9**: e1003395.
26. Ivey NS, MacLean AG, Lackner AA. Acquired immunodeficiency syndrome and the blood–brain barrier. *J Neurovirol* 2009; **15**: 111–122.
27. Zhang JR, Tuomanen E. Molecular and cellular mechanisms for microbial entry into the CNS. *J Neurovirol* 1999; **5**: 591–603.
28. Finke S, Conzelmann KK. Replication strategies of rabies virus. *Virus Res* 2005; **111**: 120–131.
29. Halevy M, Akov Y, Ben-Nathan D, Kobiler D, Lachmi B, Lustig S. Loss of active neuroinvasiveness in attenuated strains of West Nile virus: pathogenicity in immunocompetent and SCID mice. *Arch Virol* 1994; **137**: 355–370.
30. Lustig S, Danenberg HD, Kafri Y, Kobiler D, Ben-Nathan D. Viral neuroinvasion and encephalitis induced by lipopolysaccharide and its mediators. *J Exp Med* 1992; **176**: 707–712.
31. Koike S, Taya C, Kurata T *et al.* Transgenic mice susceptible to poliovirus. *Proc Natl Acad Sci U S A* 1991; **88**: 951–955.
32. Yang WX, Terasaki T, Shiroki K *et al.* Efficient delivery of circulating poliovirus to the central nervous system independently of poliovirus receptor. *Virology* 1997; **229**: 421–428.
33. Mueller SN, Hosiawa-Meagher KA, Konieczny BT *et al.* Regulation of homeostatic chemokine expression and cell trafficking during immune responses. *Science* 2007; **317**: 670–674.
34. Davis KJ, Anderson AO, Geisbert TW *et al.* Pathology of experimental Ebola virus infection in African green monkeys. Involvement of fibroblastic reticular cells. *Arch Pathol Lab Med* 1997; **121**: 805–819.
35. Steele KE, Anderson AO, Mohamadzadeh M. Fibroblastic reticular cells and their role in viral hemorrhagic fevers. *Expert Rev Anti Infect Ther* 2009; **7**: 423–435.
36. Gretz JE, Kaldjian EP, Anderson AO, Shaw S. Sophisticated strategies for information encounter in the lymph node: the reticular network as a conduit of soluble information and a highway for cell traffic. *J Immunol* 1996; **157**: 495–499.
37. Gretz JE, Anderson AO, Shaw S. Cords, channels, corridors and conduits: critical architectural elements facilitating cell interactions in the lymph node cortex. *Immunol Rev* 1997; **156**: 11–24.
38. Sixt M, Kanazawa N, Selg M *et al.* The conduit system transports soluble antigens from the afferent lymph to

resident dendritic cells in the T cell area of the lymph node. *Immunity* 2005; **22**: 19–29.
39. Nolte MA, Belien JAM, Schadee-Eestermans I *et al.* A conduit system distributes chemokines and small blood-borne molecules through the splenic white pulp. *J Exp Med* 2003; **198**: 505–512.
40. Bajenoff M, Glaichenhaus N, Germain RN. Fibroblastic reticular cells guide T lymphocyte entry into and migration within the splenic T cell zone. *J Immunol* 2008; **181**: 3947–3954.
41. Van Vliet E, Melis M, Foidart JM, Van Ewijk W. Reticular fibroblasts in peripheral lymphoid organs identified by a monoclonal antibody. *J Histochem Cytochem* 1986; **34**: 883–890.
42. Bajenoff M, Egen JG, Koo LY *et al.* Stromal cell networks regulate lymphocyte entry, migration, and territoriality in lymph nodes. *Immunity* 2006; **25**: 989–1001.
43. Lokmic Z, Lammermann T, Sixt M, Cardell S, Hallmann R, Sorokin L. The extracellular matrix of the spleen as a potential organizer of immune cell compartments. *Semin Immunol* 2008; **20**: 4–13.
44. Gretz JE, Norbury CC, Anderson AO, Proudfoot AE, Shaw S. Lymph-borne chemokines and other low molecular weight molecules reach high endothelial venules via specialized conduits while a functional barrier limits access to the lymphocyte microenvironments in lymph node cortex. *J Exp Med* 2000; **192**: 1425–1440.
45. Malhotra D, Fletcher AL, Astarita J *et al.* Transcriptional profiling of stroma from inflamed and resting lymph nodes defines immunological hallmarks. *Nat Immunol* 2012; **13**: 499–510.
46. Link A, Hardie DL, Favre S *et al.* Association of T-zone reticular networks and conduits with ectopic lymphoid tissues in mice and humans. *Am J Pathol* 2011; **178**: 1662–1675.
47. Katakai T, Hara T, Sugai M, Gonda H, Shimuzu A. Lymph node fibroblastic reticular cells construct the stromal reticulum via contact with lymphocytes. *J Exp Med* 2004; **200**: 783–795.
48. Battistella M, Guedj N, Fallet-Bianco C, Bodemer C, Brousse N, Fraitag S. The histopathological spectrum of cutaneous meningeal heterotopias: clues and pitfalls. *Histopathology* 2011; **59**: 407–420.
49. Yi JH, Katagiri Y, Susarla B, Figge D, Symes AJ, Geller HM. Alterations in sulfated chondroitin glycosaminoglycans following controlled cortical impact injury in mice. *J Comp Neurol* 2012; **520**: 3295–3313.
50. Roth-Cross JK, Bender SJ, Weiss SR. Murine Coronavirus Mouse Hepatitis Virus Is Recognized by MDA5 and Induces Type I Interferon in Brain Macrophages/Microglia. *J Virol* 2008; **82**: 9829–9838.
51. Woollam D, Millen J. Vascular tissues in the central nervous system. In: Minckler J, ed. Pathology of the Nervous System, vol. **1**. New York: McGraw-Hill Education, 1968; 491–498.
52. Wilson EH, Harris TH, Mrass P *et al.* Behavior of parasite-specific effector CD8+ T cells in the brain and visualization of a kinesis-associated system of reticular fibers. *Immunity* 2009; **30**: 300–311.
53. Kim JV, Kang SS, Dustin ML, McGavern DB. Myelomonocytic cell recruitment causes fatal CNS vascular injury during acute viral meningitis. *Nature* 2009; **457**: 191–195.
54. Takahashi H, Kanesaki H, Igarashi T *et al.* Reactive gliosis of astrocytes and Muller glial cells in retina of POMGnT1-deficient mice. *Mol Cell Neurosci* 2011; **47**: 119–130.
55. Rotbart HA, Brennan PJ, Fife KH *et al.* Enterovirus meningitis in adults. *Clin Infect Dis* 1998; **27**: 896–898.
56. Price RA, Garcia JH, Rightsel WA. Choriomeningitis and myocarditis in an adolescent with isolation of coxsackie B-5 virus. *Am J Clin Pathol* 1970; **53**: 825–831.
57. Irani DN. Aseptic meningitis and viral myelitis. *Neurol Clin* 2008; **26**: 635–55 vii-viii.
58. Heck N, Garwood J, Dobbertin A *et al.* Evidence for distinct leptomeningeal cell-dependent paracrine and EGF-linked autocrine regulatory pathways for suppression of fibrillar collagens in astrocytes. *Mol Cell Neurosci* 2007; **36**: 71–85.
59. Ame-Thomas P, Maby-El Hajjami H, Monvoisin C *et al.* Human mesenchymal stem cells isolated from bone marrow and lymphoid organs support tumor B-cell growth: role of stromal cells in follicular lymphoma pathogenesis. *Blood* 2007; **109**: 693–702.
60. Bonkowski D, Katyshev V, Balabanov RD, Borisov A, Dore-Duffy P. The CNS microvascular pericyte: pericyte-astrocyte crosstalk in the regulation of tissue survival. *Fluids Barriers CNS* 2011; **8**: 8.
61. Griffiths GM, Tsun A, Stinchcombe JC. The immunological synapse: a focal point for endocytosis and exocytosis. *J Cell Biol* 2010; **189**: 399–406.
62. Rostene W, Kitabgi P, Parsadaniantz SM. Chemokines: a new class of neuromodulator? *Nat Rev Neurosci* 2007; **8**: 895–903.
63. Biber K, Neumann H, Inoue K, Boddeke HW. Neuronal 'On' and 'Off' signals control microglia. *Trends Neurosci* 2007; **30**: 596–602.

SUPPORTING INFORMATION

Additional supporting information may be found in the online version of this article at the publisher's web site:

Supplemental Figure S1. Immunofluorescence to detect ERag (Er), laminin (La), JHMV (V), Zic2, podoplanin (Pod), GFAP (Gf), CD11b, NeuN and nucleus (Nuc). Images were taken in areas of the peripheral nerve (PN) or

CNS region in the trigeminal root (TrigR), fourth ventricle (IVv), meninx (Mx), inferior cerebellar peduncle (ICP), and pons (Po). Figure (Fig.) numbers in parenthesis indicate the figures where the legend of each image is described. Long arrows and arrowheads in E indicate $CD11b^{high}$ and $CD11b^{low}$ cells, respectively. J: The area of the trigeminal root in Figure 1A, which is indicated by the boxed area, is indicated by closed lines. The border between the CNS area (upper right) and peripheral nerve (lower left) is indicated by a dotted line. Single and double bars indicate 50 and 20 μm, respectively.

Supplemental Figure S2. Infiltrating cells indicated by nuclear staining (blue) between thin sheets with collagen III (red) and ERag (green), illustrated in Figure 4B, are viewed from different angles. Bar indicates 10 μm.

Supplemental Movie S1. Supporting info item

Supplemental Movie S2. Supporting info item